Journal of Materials Chemistry A

PAPER

Cite this: J. Mater. Chem. A, 2014, 2, 12232

Nitrogen and sulfur co-doped graphene counter electrodes with synergistically enhanced performance for dye-sensitized solar cells†

Aravindaraj G. Kannan,[a] Jinxing Zhao,[a] Sung Geun Jo,[a] Yong Soo Kang[b] and Dong-Won Kim*[a]

Received 18th April 2014
Accepted 2nd June 2014

DOI: 10.1039/c4ta01927j

www.rsc.org/MaterialsA

A highly efficient nitrogen and sulfur co-doped graphene (NSG) nanosheet for dye-sensitized solar cells (DSSCs) was synthesized using a simple hydrothermal method, and its electrocatalytic activity towards the I_3^-/I^- redox reaction was investigated. The NSG materials showed a uniform distribution of nitrogen and sulfur heteroatoms throughout the graphene nanosheet. The doped nitrogen was present in the form of pyridinic, pyrrolic and graphitic states, and the doped sulfur was present in the C–S–C configuration. The DSSC with the NSG counter electrode exhibited a high conversion efficiency (7.42%), similar to that of the Pt counter electrode (7.56%) and much higher than that of the only N- or S-doped graphene electrodes. The high catalytic activity of the NSG electrode is attributed to the synergistic effect of the high charge polarization arising from the difference in electronegativity between nitrogen and carbon as well as the structural distortion caused by the bigger atomic size of the sulfur atom. To the best of our knowledge, the synergistic effect of co-doping of graphene on the counter electrode performance in DSSCs is demonstrated for the first time, and co-doping is proposed as a promising approach to enhance the photovoltaic performance of DSSCs.

Introduction

Dye-sensitized solar cells (DSSCs) have attracted great attention due to their inherent advantages such as low cost, easy fabrication and relatively high conversion efficiency.[1] DSSCs consist of a dye-sensitized TiO_2 electrode, an electrolyte containing a redox couple and a counter electrode. The counter electrode is a crucial component that plays a critical role in the regeneration of oxidized ionic species in the electrolyte. Platinum has been widely used as a counter electrode in DSSCs due to its high catalytic activity for I_3^- reduction and high electronic conductivity. However, it is expensive, scarce and unstable in a highly corrosive electrolyte containing I^-/I_3^- redox species. Hence, the noble Pt metal should be replaced with cost-effective and corrosion-resistant alternatives in order to achieve commercial success. The ideal alternative counter electrode should have good electrocatalytic activity, large surface area, high electronic conductivity, high stability in the corrosive electrolyte and be abundantly available. Several materials such as conducting polymers,[2,3] inorganic metal compounds[4] and carbon-based materials[5,6] have been actively explored as alternative counter electrodes. Among these materials, carbon-based materials such as carbon nanotubes, amorphous carbon and graphene nanosheets show promising properties as Pt-free counter electrodes.[6–8] Graphene nanosheets with a two-dimensional, sp^2-hybridized carbon structure possess many superior properties, such as high electronic conductivity, high surface area, chemical stability and good mechanical strength, and have emerged as a promising material for counter electrodes among the carbon-based materials.[9–15] Roy-Mayhew *et al.*[16] demonstrated that the defect sites created by the oxygen functional groups in graphene oxide act as catalytic centers for the reduction of I_3^- species in the electrolyte. However, the introduction of defect sites by oxygen functional groups destroys the conductive carbon network, thereby reducing the electronic conductivity of graphene nanosheets. Recently, to obtain high catalytic activity without reducing the electrical conductivity of graphene, heteroatoms such as nitrogen[17–21] and boron[22] have been doped into graphene. Among the heteroatoms doped in graphene, nitrogen is by far the most prominent doping element and it induces structural deformation due to the local strains in the carbon framework. The lone-pair of electrons of nitrogen can also induce negative charge with respect to the delocalized,

[a]Department of Chemical Engineering, Hanyang University, Seoul 133-791, Republic of Korea. E-mail: dongwonkim@hanyang.ac.kr; Fax: +82 2 2298 4101; Tel: +82 2 2220 2337

[b]Department of Energy Engineering, Hanyang University, Seoul 133-791, Republic of Korea

† Electronic supplementary information (ESI) available: TEM images of NG and SG control samples; XPS survey spectra of NG, SG, NSG and GO nanosheets; FT-IR spectrum of the NSG sample; XRD patterns of graphite, GO and NSG samples; photocurrent density–voltage curves of DSSCs with NSG counter electrodes of different thicknesses; CVs of NSG, SG, NG and rGO samples. See DOI: 10.1039/c4ta01927j

sp^2-hybridized carbon framework, resulting in enhanced electron transfer ability as well as improved electrocatalytic activity.[21] Doping with additional heteroatoms has been known to synergistically enhance the electrocatalytic activity of graphene nanosheets due to the increased asymmetries of charge and spin densities at the different sites of the dual-doped materials.[23–25] It is thus expected that such dual-doped graphene sheets would be promising to replace the expensive Pt counter electrode in DSSCs. To the best of our knowledge, graphene nanosheets co-doped with two heteroatoms have not been explored as counter electrodes in DSSCs so far.

In the present study, we synthesized N and S dual-doped graphene (hereafter referred to as NSG) nanosheets using a simple, single-step hydrothermal method, as schematically illustrated in Fig. 1, and we explored this material as a counter electrode for DSSCs. Nitrogen and sulfur heteroatoms were chosen as dopants due to their higher electronegativity and bigger atomic size in comparison to carbon atoms, properties that result in structural as well as charge and spin density modifications of graphene for better electrocatalytic activity. The DSSC assembled with the NSG electrode exhibited a high conversion efficiency of 7.42%, which was higher than those of the DSSCs with counter electrodes fabricated using N-doped (NG) or S-doped (SG) graphene due to the synergistic effect of the dual-doped heteroatoms.

Experimental

Materials synthesis

Graphite oxide was prepared using the modified Hummer's method from graphite powder (SP-1, 30 μm nominal particle size, Bay Carbon, USA). Pre-oxidation of graphite was carried out as reported by Kovtyukhova *et al.*,[26] followed by oxidation using the Hummers method.[27] The graphite oxide was ultrasonicated to exfoliate individual graphene oxide (GO) sheets. The NSG sample was prepared by a simple hydrothermal method using thiourea as a source for both nitrogen and sulfur heteroatoms. Here, thiourea also acts as a reducing agent for the partial reduction of GO. In a typical synthesis, 300 mg of GO was dispersed in 70 mL DI water, and 900 mg of thiourea was added to the solution and stirred for 4 h. Then the reaction mixture was transferred into a Teflon-lined stainless steel autoclave and maintained at 180 °C for 12 h, after which, the autoclave was allowed to cool down naturally. The resulting gel was alternatively washed with DI water and ethanol, and then dried overnight at room temperature in a vacuum oven. The samples were further reduced at 700 °C in an Ar atmosphere for 1 h and then used for further characterization and performance evaluation. SG and NG control samples were prepared using similar preparation conditions with thiophene and urea as sources of nitrogen and sulfur, respectively. An undoped reduced graphene oxide (rGO) control sample was also prepared by reducing GO using hydrazine monohydrate.

Characterization

The morphology of the NSG sample was characterized using scanning electron microscopy (SEM, JEOL JSM 6701F) and transmission electron microscopy (TEM, JEOL JEM 2100F). The distribution of the doped heteroatoms on graphene was examined using electron energy loss spectroscopy (EELS) mapping. The amount of doping and the nature of chemical changes caused by N,S co-doping were analyzed using X-ray photoelectron spectroscopy (XPS, VG multilab ESCA system, 220i). Fourier transform infrared (FT-IR) spectra were recorded on a JASCO 460 IR spectrometer in the range of 500–4000 cm^{-1} with KBR powder-pressed pellets. The NSG sample was further characterized using Raman spectroscopy (Dongwoo optron, MonoRa 780i) to understand its structure and to investigate the graphene quality. Nitrogen adsorption/desorption isotherms were recorded using an Autosorb-IQ MP (Quantachrome INC.) apparatus at 77 K and the sample was degassed at 100 °C for 3 h prior to measurement.

DSSC fabrication

The NSG-based counter electrode was prepared by electrospraying NSG solution (0.05 wt% solution uniformly dispersed

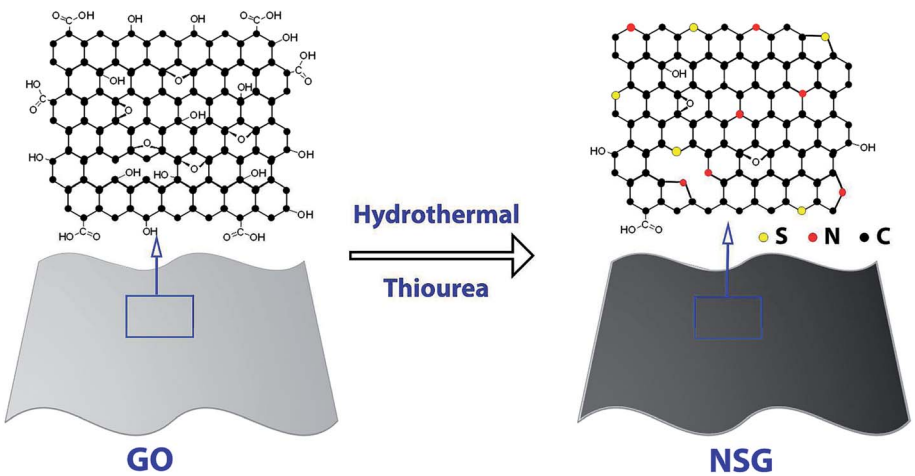

Fig. 1 Schematic illustration of the synthesis of NSG nanosheets from GO and thiourea using a simple hydrothermal method.

in ethanol) onto the FTO glass. A voltage of 10 kV was applied between the metallic orifice and the substrate, with a distance of 4.5 cm from the substrate to the metallic orifice. NG, SG and rGO control samples were also deposited onto FTO glass by the electro-spray technique. The electro-sprayed electrodes were annealed at 300 °C for 30 min in an Ar atmosphere. The thickness of the NSG-based counter electrode was optimized to be 800 nm. The Pt-based counter electrode was prepared by spin coating 0.01 M H_2PtCl_6 in isopropanol onto the FTO substrate and sintering at 450 °C for 1 h. Nanocrystalline TiO_2 paste (Ti-Nanoxide T20/SP, Solaronix) was cast onto FTO glass with a doctor blade and sintered at 450 °C for 30 min. Its thickness was optimized to be 12 μm. An active area of 0.25 cm^2 was selected from a sintered TiO_2 electrode and sensitized overnight in a *cis*-diisothiocyanato-bis(2,2′-bipyridyl-4,4′-dicarboxylato) ruthenium(II) bis(tetrabutyl ammonium) (Ruthenium 535 bis-TBA, Solaronix) dye solution. DSSCs were fabricated by sealing the TiO_2 electrode and counter electrode together using a hot melting film (Solarnix SA, SX1170 hot melt). The liquid electrolyte was then injected into the cell through a hole in the counter electrode. The electrolyte solution used was 0.5 M lithium iodide, 0.05 M I_2 and 0.5 M 4-*tert*-butylpyridine dissolved in acetonitrile. The photovoltaic performance of the DSSCs was evaluated using a xenon light source (100 mW cm^{-2}) with an AM 1.5 filter in a solar simulator. The light intensity was calibrated with a NREL-calibrated Si solar cell (PV Measurements, Inc.). A black mask with a 0.25 cm^2 aperture was placed over the cells during irradiation, and an anti-reflection glass was placed on the front glass cover over the cells.

Electrochemical measurements

Cyclic voltammetric (CV) measurements of NSG-, Pt-, SG-, NG- and rGO-based electrodes were carried out using a potentiostat (Zahner Electrik IM6) in a three-electrode configuration with an Ag/Ag^+ reference electrode (3 M KCl solution) and Pt wire as a counter electrode. The electrolyte was prepared by dissolving 0.5 mmol lithium iodide, 0.5 mmol iodine and 0.1 mol lithium perchlorate in acetonitrile. The potential range was −0.50 to 0.60 V with a scan rate of 50 mV s^{-1}. AC impedance measurements of the symmetric cell with two identical electrodes were performed using a Zahner Electrik IM6 impedance analyzer over the frequency range of 50 mHz to 500 kHz with an amplitude of 10 mV at open circuit potential. Tafel polarization curves were obtained using symmetric cells in the potential range of ±1 V.

Results and discussion

The simple and low-temperature synthesis of NSG nanosheets *via* a hydrothermal method is schematically illustrated in Fig. 1. During the hydrothermal treatment, thiourea is thermally decomposed into ammonia, hydrogen sulfide, isothiocyanic acid and carbodiimide.[28,29] The resulting ammonia and hydrogen sulfide act as sources of nitrogen and sulfur, respectively, during the heteroatom doping process.[30,31] The oxygen-containing functional groups in GO react with ammonia and hydrogen sulfide to form C–N and C–S bonds, respectively. Generally, such reactions require high temperature and inert/vacuum conditions, but our synthetic method uses a relatively lower temperature of 180 °C. Thiourea can simultaneously act as a reducing agent of GO.[32] The simultaneous process of dual-doping and GO reduction is very simple and uses commonly available chemicals, which makes it suitable for industrial-scale applications. The control samples, SG and NG, were prepared using the same procedure by replacing thiourea with thiophene and urea, respectively. An rGO sample without any doping was also prepared for comparison.

The morphology of the dual-doped NSG sample (Fig. 2a and b) shows a highly folded structure, which is attributed to the relatively larger atomic size of the sulfur atom (1.02 Å) compared with the carbon atom (0.77 Å). The additional doping of larger heteroatoms (such as sulfur) creates a high curvature on the carbon surface, which results in highly wrinkled and curved morphologies, as reported previously.[31,33] The resulting loosely packed structure (as observed in Fig. 2a) produces voids between the adjacent doped graphene sheets, which facilitate the easy access of electrolytes to the catalytic surface. From the NSG folded area (shown in Fig. 2c), we can observe that less than 10 layers of dual-doped graphene are present in the sample. The NG and SG control samples also show the highly folded morphology (ESI, Fig. S1†), similar to the NSG sample. The typical nitrogen adsorption/desorption curve of the NSG sample (Fig. 2d) exhibits a type IV adsorption isotherm with a sharp capillary condensation step and a type 2 hysteresis loop (IUPAC classification), which imply the existence of a large number of mesopores in the structure with an average pore size

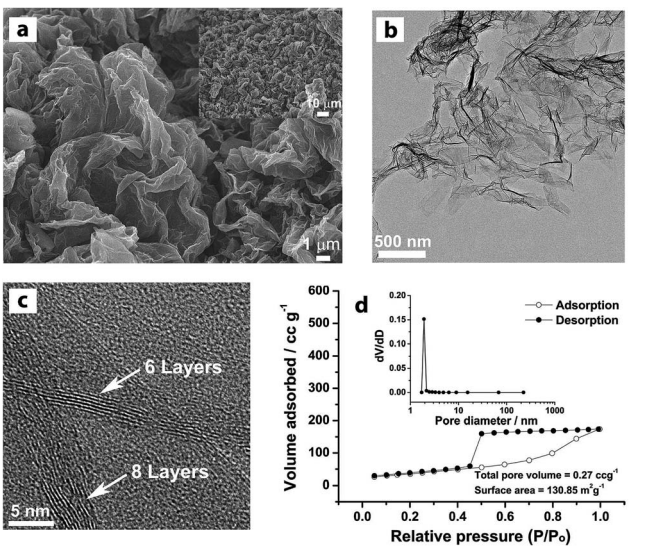

Fig. 2 (a) SEM and (b) TEM images of NSG nanosheets showing highly folded morphology due to the structural defects induced by the co-doping of heteroatoms. The inset in (a) shows a low-magnification SEM image of NSG nanosheets. (c) HR-TEM image of an NSG nanosheet showing the folded regions. (d) Nitrogen adsorption/desorption isotherms of the NSG sample. The inset shows that the pore size of the NSG sample was ~2 nm, implying that the NSG sample has a mesoporous structure.

of 2 nm. The Brunauer–Emmet–Teller (BET) surface area of the NSG sample is estimated to be about 130 $m^2 g^{-1}$ with a mesopore volume of 0.27 $cm^3 g^{-1}$, which is significantly lower than the theoretical surface area of 2630 $m^2 g^{-1}$ for an individual, isolated graphene sheet, indicating the presence of more than one layer of graphene sheets in the sample.[34] The mesoporous structure may facilitate the easy transport of the redox couple in the electrolyte to the catalytic active sites in the NSG electrode.

The elemental mapping of the NSG sample (Fig. 3) shows a uniform distribution of nitrogen, sulfur and carbon atoms throughout the graphene nanosheets and that the doped elements are present both in the basal plane as well as in the edges of graphene. XPS analysis was performed to investigate the chemical nature and the heteroatom bonding configurations. The XPS spectrum of the NSG sample (ESI, Fig. S2†) shows the successful incorporation of N and S heteroatoms, and the amounts of nitrogen and sulfur in the NSG sample are measured to be 2.02 atomic% and 2.54 atomic%, respectively. In addition, the calculated C/O ratios of NSG and GO samples from the XPS spectra are 9.75 and 1.91, respectively. These results suggest that the oxide groups in the graphene nanosheets are highly reduced during the co-doping process. In the case of the NG and SG samples, the peaks corresponding to N 1s and S 2p are observed, respectively, in addition to C 1s and O 1s peaks. This confirms the successful incorporation of just sulfur or nitrogen atoms into the graphene framework. The amount of sulfur doping and the C/O ratio in the SG sample are estimated to be 2.71 atomic%, and 9.42, respectively, whereas the NG sample contains 2.96 atomic% nitrogen with a C/O ratio of 9.58. The amount of heteroatom doping and the C/O ratio of the control samples are comparable to those of the NSG sample, thereby demonstrating that the performance of these materials can be easily compared.

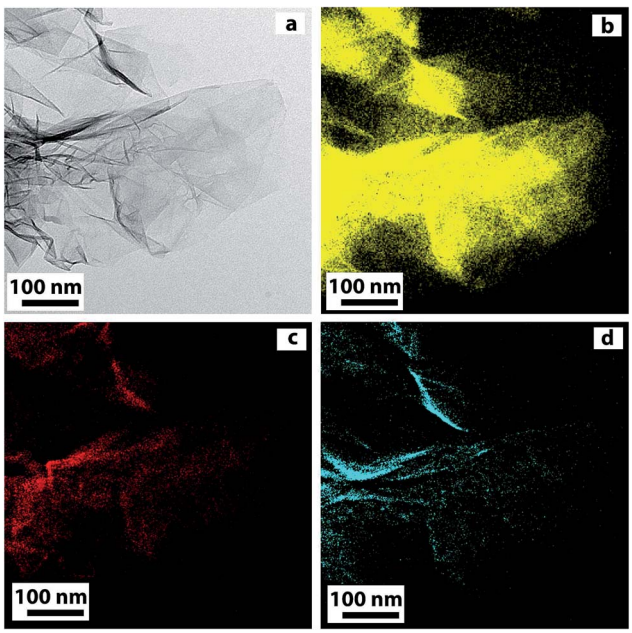

Fig. 3 Elemental mapping of NSG nanosheets: (a) TEM image, (b) C mapping, (c) S mapping and (d) N mapping.

The N 1s peak in the high-resolution XPS spectrum was resolved into three peaks at 397.6, 399.8 and 401.5 eV, as shown in Fig. 4a, which are attributed to pyridinic-, pyrrolic- and graphitic-type nitrogen, respectively.[35,36] The pyridinic and pyrrolic N are located at the edge of the graphene sheets or in the defect sites present in the basal plane and are bonded to two adjacent carbon atoms. On the other hand, the graphitic N is present both at the edges and in the basal plane replacing a carbon atom in the carbon framework.[37] Hou *et al.* reported that the state of nitrogen in N-doped graphene determined its catalytic activity.[21] Among the three types of nitrogen, pyridinic and graphitic N provide highly active sites due to the shift in redox potential as well as lowered absorption energy. The relative ratio of nitrogen states was determined based on the area of the deconvoluted curves, and the NSG sample contained 14, 50 and 36% of pyridinic, pyrrolic and graphitic N, respectively. As reported in previous literature utilizing similar annealing conditions,[21] pyrrolic N dominated in the NSG sample. The S 2p peak shown in Fig. 4b could be also deconvoluted into three peaks. The peaks at 163.6 and 164.8 eV correspond to sulfur atoms bound in aromatic carbon structures, and the peak at a higher binding energy represents C–SO_x states,[38–40] which is only 8% of the total sulfur present in the sample. This result demonstrates that the doped sulfur is predominantly incorporated in the carbon framework and only a small amount of oxidized sulfur species is present in the NSG sample. The deconvolution of the C1s peak (Fig. 4c) shows the presence of three peaks. The peak at 284.5 eV confirms the presence of sp^2-hybridized carbon, and the peak at 285.4 eV indicates the presence of C–O, C–S and C–N.[41,42] The peak at 288.8 eV is attributed to C=O, demonstrating the presence of residual carbonyl and carboxyl groups. FT-IR spectroscopy (ESI, Fig. S3†) was used to identify the surface functional groups present in the NSG sample. The FT-IR spectrum provided evidence for the presence of C–O, C–N, C–S, C=O and C=C groups. These

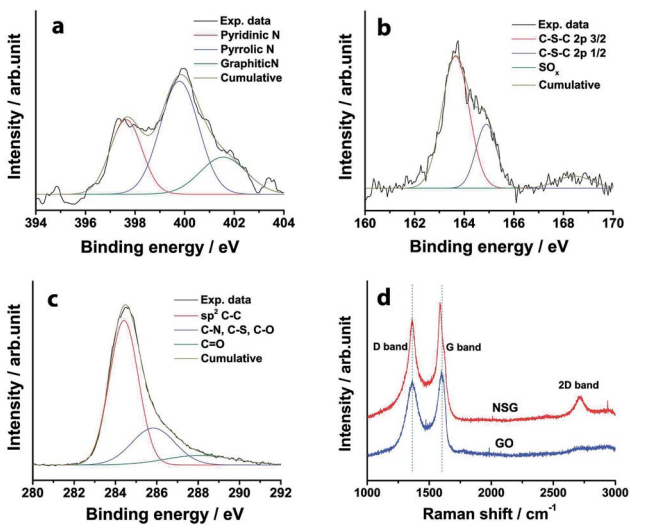

Fig. 4 High-resolution XPS spectra of (a) N 1s, (b) S 2p and (c) C 1s of NSG nanosheets. (d) Raman spectra of GO and NSG samples showing the presence of G, D and 2D bands.

results confirm the doping of nitrogen as well as sulfur in the carbon framework. The NSG sample was further characterized using Raman spectroscopy to understand its structure and quality. Raman spectra of GO and NSG samples shown in Fig. 4d show the characteristic D and G bands. The D band is located at ~1355 cm^{-1} and is induced by the local basal plane derivatization that creates sp^3 distortion.[43] The G band arising from the sp^2-hybridized graphitic carbon atoms is more red-shifted to 1587 cm^{-1} in comparison to the GO sample (around 1600 cm^{-1}). This red-shift is an important characteristic of n-type substitutional doping of graphene, as reported in previous literature.[39,44,45] This result confirms the doping of sulfur and nitrogen atoms in the graphene structure. Moreover, the broad 2D band observed at 2700 cm^{-1} in the NSG sample indicates the predominant presence of a mixture of single- and few-layer graphene sheets.[46,47] The presence of well-exfoliated samples was further confirmed with X-ray diffraction (XRD) measurements (ESI, Fig. S4†). The diffraction pattern of graphite shows a sharp peak at 26° corresponding to a *d*-layer spacing of 0.34 nm, and the GO diffraction pattern shows a strong peak at 10.5° corresponding to an inter-layer spacing of 0.84 nm. In contrast, the diffraction pattern of the NSG sample exhibits a very broad and low-intensity peak at 24.4°, suggesting the re-stacking of a negligible amount of doped graphitic sheets through π–π interactions and the predominant presence of well-exfoliated graphene nanosheets.[48] These results further substantiate the HRTEM results, which demonstrated the presence of few-layer graphene sheets.

To evaluate the performance of the prepared materials as counter electrodes in DSSCs, they were dispersed in ethanol and deposited on a fluorine-doped tin oxide (FTO) glass using the electro-spray technique.[19] The NSG sample coated on the FTO glass shows a macroporous morphology with a random arrangement of graphene nanosheets, as shown in Fig. 5a. The thickness of the NSG counter electrode was controlled by varying the electrospraying duration, and the optimum thickness of the electrode was determined based on the photovoltaic performance of DSSCs. The photocurrent density–voltage curves of the DSSCs with different NSG electrode thicknesses are shown in Fig. S5.† The optimum thickness of the NSG layer was determined to be about 800 nm for achieving the highest conversion efficiency, and the optimum thickness was used for further evaluation of electrocatalytic properties as well the photovoltaic performance of all the electrodes. A cross-sectional SEM image of the optimized NSG electrode is given in Fig. 5b, which shows that the coating layer is well-adhered to the FTO glass and is uniform throughout the electrode. This result suggests that electrospraying is a very effective technique to prepare the counter electrodes for DSSCs. The inherent mesoporosity in the NSG sample along with the formed macroporous structure is expected to enhance the contact between the catalytic sites and the electrolyte solution.

Before comparing the photovoltaic performance of the NSG sample with other control samples, the catalytic activity was evaluated by CV measurements using a three-electrode configuration (Fig. 6a and S6†). As shown in the figure, the NSG sample and control samples all show a pair of redox peaks at approximately −0.05 and 0.39 V (all potentials are given with respect to an Ag/AgCl reference electrode), which correspond to the redox reaction of $I_3^- + 2e^- \leftrightarrow 3I^-$.[49] These results demonstrate that the graphene-based samples are active catalysts for the reduction of triiodide to iodide. The catalytic activity of different counter electrodes can be compared by determining the peak current density (J_p) and the peak–peak separation of the redox peaks (ΔE), where a higher peak current density and a smaller ΔE indicate better catalytic activity of the electrode. Among the graphene-based samples, the NSG sample showed the highest peak current density and the smallest ΔE, indicating that the dual-doped sample effectively reduced the triiodide species in the electrolyte. For example, the NSG sample demonstrated ΔE and J_p values of 0.45 V and 1.10 mA cm^{-2}, respectively, whereas the best sample (SG) among the control samples demonstrated ΔE and J_p values of 0.51 V and 0.98 mA cm^{-2}, respectively. In comparison, the Pt counter electrode

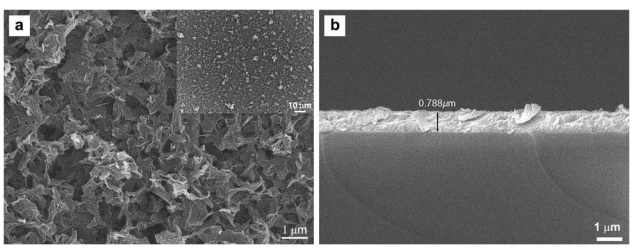

Fig. 5 (a) A representative SEM image of the NSG counter electrode electrosprayed on a FTO glass and the inset shows the low-magnification SEM image. (b) Cross-sectional SEM image of the NSG counter electrode.

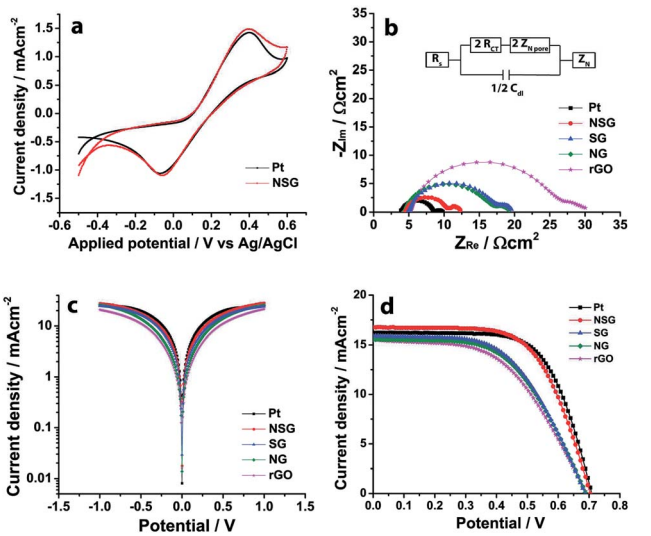

Fig. 6 (a) CV curves of NSG and Pt electrodes obtained at a scan rate of 50 mV s^{-1} using Pt wire and Ag/Ag^+ as counter and reference electrodes, respectively. (b) Nyquist plots of different counter electrodes using symmetric cells. (c) Tafel polarization curves of different counter electrodes using symmetric cells. (d) Photocurrent–voltage curves of DSSCs with different counter electrodes under one-sun illumination.

Table 1 Photovoltaic performance of DSSCs with different counter electrodes, and electrochemical parameters measured from EIS data and Tafel plots[a]

Counter electrode	J_{sc} (mA cm^{-2})	V_{oc} (V)	FF	η (%)	R_{ct} (Ω cm^2)	R_c (Ω cm^2)	j_o (mA cm^{-2})
Pt	16.21	0.71	66.08	7.58	2.73	22.87	8.39
rGO	15.57	0.69	51.70	5.57	10.66	54.63	3.78
NG	15.54	0.69	54.90	5.89	6.05	50.77	3.69
SG	15.89	0.69	54.85	6.00	5.91	36.07	5.57
NSG	16.78	0.70	62.77	7.42	2.82	28.50	6.19

[a] (R_{ct} from EIS data; R_c and j_o from Tafel plots).

exhibits ΔE and J_p values of 0.46 V and 1.06 mA cm^{-2}, respectively. The electrocatalytic activity of the graphene-based electrodes was found to be quite stable in liquid electrolytes. To further investigate the electro-catalytic activity of the prepared samples, electrochemical impedance spectroscopy (EIS) measurements were carried out using symmetric cells (Fig. 6b). All the cells show two distinct semicircles in the high- and low-frequency regions, which correspond to the charge transfer process and the Nernst diffusion process, respectively. The spectra were fitted with an equivalent circuit shown in the inset of Fig. 6b, and the corresponding values are given in Table 1. The NSG-based counter electrode shows an R_{ct} value of 2.82 Ω cm^2, which is almost identical to that of the Pt-based counter electrode (2.73 Ω cm^2) and much lower than those of the other control samples. The R_{ct} value of the NSG-based counter electrode is smaller by a factor of more than three in comparison to the rGO-based electrode and is almost half that of the NG (6.05 Ω cm^2) and SG electrodes (5.91 Ω cm^2). The charge transfer resistance at the counter electrode–electrolyte interface is a critical parameter that indicates the effectiveness of the counter electrode in regenerating the iodine species in the electrolyte. A lower R_{ct} value indicates the enhanced reduction of triiodide ions at the counter electrode–electrolyte interface, thereby increasing the availability of I^- ions at the dye–electrolyte interface. This could result in the suppression of charge recombination in the photoanode, resulting in an increase in the open circuit voltage of the DSSCs.[50,51] Tafel polarization curves were obtained for all samples using symmetric cells in the potential range of −1 to 1 V, as shown in Fig. 6c. The slope at a potential of ∼0 V could be used to evaluate the overall resistance of the cell.[19] The overall cell resistances (R_c) of Pt, NSG, SG, NG and rGO-based cells were measured to be 22.87, 28.50, 36.07, 50.77 and 54.63 Ω cm^2, respectively. The exchange current densities (j_o) calculated from the intersection of linear anodic and cathodic curves are also presented in Table 1, revealing the same trend as the R_{ct} and R_c values and further confirming the better catalytic activity of the NSG sample in comparison to single-heteroatom-doped (NG and SG) samples as well as the undoped (rGO) sample. The photocurrent density–voltage curves of the DSSCs assembled with different counter electrodes are shown in Fig. 6d and the values of J_{sc}, OCV, FF and η are given in Table 1. The DSSC with the NSG-based counter electrode clearly exhibited the highest J_{sc} (16.78 mA cm^{-2}), FF (62.77) and η (7.42%) among the graphene-based cells; these values are similar to those of a DSSC with a Pt-based counter electrode. The photovoltaic performance of DSSCs with graphene-based counter electrodes is in the order of NSG > SG > NG > rGO. This result suggests that the doping of graphene with heteroatoms enhances the electrocatalytic activity in the counter electrode, which results in higher J_{sc} and FF, thereby resulting in higher conversion efficiency. Furthermore, the NSG electrode showed enhanced performance in comparison to the NG and SG electrodes due to the synergistic effect of co-doping of the graphene nanosheets. This is the first work reporting the synergistic effects of the co-doping of graphene with two heteroatoms for counter electrodes in DSSCs. The presence of heteroatoms, including nitrogen, in the graphene nanosheets breaks the charge neutrality of the graphitic carbon and favors the adsorption to and subsequent reduction of triiodide on the surrounding carbon atoms. Density functional theory (DFT) calculations by Zhang *et al.* showed that the spin density plays a more important role than the atomic charge density in determining the catalytic active sites.[52] In another study based on DFT calculations, Liang *et al.* reported that the co-doping of N and S atoms on graphene nanosheets substantially enhanced the asymmetric spin density as well as the charge density, which are responsible for the electrocatalytic activities.[24] Thus, the enhanced electrocatalytic performance of the NSG-based counter electrodes in DSSCs can be attributed to the synergistic effect of nitrogen and sulfur co-doping in the graphene structure.

Conclusions

Nitrogen and sulfur co-doped graphene nanosheets were successfully synthesized by using a simple hydrothermal method and were evaluated for the first time as counter electrodes in DSSCs. The NSG sample showed a uniform distribution of doped heteroatoms throughout the sample, and the dual-doped graphene nanosheets had a highly wrinkled and curved morphology. The NSG-based electrode prepared using the electrospray technique exhibited high electro–catalytic activity towards the I_3^-/I^- redox couple as evidenced from the lower charge transfer resistance, which is smaller by a factor of 2–4 compared to NG, SG and rGO samples. Co-doping of N and S heteroatoms synergistically enhanced the photovoltaic performance of DSSCs with a NSG-based counter electrode, which is similar to that of the DSSC with a Pt-based counter

electrode. Based on these results, the co-doping of heteroatoms synergistically enhanced the asymmetric spin and charge densities of carbon atoms that are responsible for superior electro-catalytic activity. It is thus suggested that co-doping of graphene with two or more heteroatoms could be an effective approach, along with electrode/device optimization, to improve the photovoltaic performance of cost-effective DSSCs.

Acknowledgements

This work was supported by the National Research Foundation of Korea (NRF) grant funded by the Korea government (MSIP) for the Center for Next Generation Dye-sensitized Solar Cells (no. 2008-0061903), and a grant from the Human Resources Development Program of KETEP funded by the Korea government Ministry of Trade, Industry and Energy (no. 20124010203290).

References

1 M. Gratzel, *Nature*, 2001, **414**, 338–344.
2 Q. Tai, B. Chen, F. Guo, S. Xu, H. Hu, B. Sebo and X.-Z. Zhao, *ACS Nano*, 2011, **5**, 3795–3799.
3 N. Jeon, D. K. Hwang, Y. S. Kang, S. S. Im and D. W. Kim, *Electrochem. Commun.*, 2013, **34**, 1–4.
4 X. Chen, Y. Hou, B. Zhang, X. H. Yang and H. G. Yang, *Chem. Commun.*, 2013, **49**, 5793–5795.
5 T. Chen, L. Qiu, Z. Cai, F. Gong, Z. Yang, Z. Wang and H. Peng, *Nano Lett.*, 2012, **12**, 2568–2572.
6 W. Kwon, J.-M. Kim and S.-W. Rhee, *J. Mater. Chem. A*, 2013, **1**, 3202–3215.
7 F. Hao, P. Dong, Q. Luo, J. B. Li, J. Lou and H. Lin, *Energy Environ. Sci.*, 2013, **6**, 2003–2019.
8 W. Hong, Y. Xu, G. Lu, C. Li and G. Shi, *Electrochem. Commun.*, 2008, **10**, 1555–1558.
9 A. K. Geim and K. S. Novoselov, *Nat. Mater.*, 2007, **6**, 183–191.
10 H. Wang and Y. H. Hu, *Energy Environ. Sci.*, 2012, **5**, 8182–8188.
11 H. Wang, K. Sun, F. Tao, D. J. Stacchiola and Y. H. Hu, *Angew. Chem., Int. Ed.*, 2013, **52**, 9210–9214.
12 H. J. Ahn, I. H. Kim, J. C. Yoon, S. I. Kim and J. H. Jang, *Chem. Commun.*, 2014, **50**, 2412–2415.
13 C. Huang, C. Li and G. Shi, *Energy Environ. Sci.*, 2012, **5**, 8848–8868.
14 C. Yang, H. Bi, D. Wan, F. Huang, X. Xie and M. Jiang, *J. Mater. Chem. A*, 2013, **1**, 770–775.
15 Y. Xu, H. Bai, G. Lu, C. Li and G. Shi, *J. Am. Chem. Soc.*, 2008, **130**, 5856–5857.
16 J. D. Roy-Mayhew, D. J. Bozym, C. Punckt and I. A. Aksay, *ACS Nano*, 2010, **4**, 6203–6211.
17 X.-K. Kong, C.-L. Chen and Q.-W. Chen, *Chem. Soc. Rev.*, 2014, **43**, 2841–2857.
18 I.-Y. Jeon, H.-J. Choi, M. J. Ju, I. T. Choi, K. Lim, J. Ko, H. K. Kim, J. C. Kim, J.-J. Lee, D. Shin, S.-M. Jung, J.-M. Seo, M.-J. Kim, N. Park, L. Dai and J.-B. Baek, *Sci. Rep.*, 2013, **3**, 2260.
19 M. J. Ju, J. C. Kim, H.-J. Choi, I. T. Choi, S. G. Kim, K. Lim, J. Ko, J.-J. Lee, I.-Y. Jeon, J.-B. Baek and H. K. Kim, *ACS Nano*, 2013, **7**, 5243–5250.
20 Y. Xue, J. Liu, H. Chen, R. Wang, D. Li, J. Qu and L. Dai, *Angew. Chem., Int. Ed.*, 2012, **51**, 12124–12127.
21 S. Hou, X. Cai, H. Wu, X. Yu, M. Peng, K. Yan and D. Zou, *Energy.Environ. Sci.*, 2013, **6**, 3356–3362.
22 H. Fang, C. Yu, T. Ma and J. Qiu, *Chem. Commun.*, 2013, **50**, 3328.
23 C. H. Choi, M. W. Chung, H. C. Kwon, S. H. Park and S. I. Woo, *J. Mater. Chem. A*, 2013, **1**, 3694–3699.
24 J. Liang, Y. Jiao, M. Jaroniec and S. Z. Qiao, *Angew. Chem., Int. Ed.*, 2012, **51**, 11496–11500.
25 J. P. Paraknowitsch and A. Thomas, *Energy Environ. Sci.*, 2013, **6**, 2839–2855.
26 N. I. Kovtyukhova, P. J. Ollivier, B. R. Martin, T. E. Mallouk, S. A. Chizhik, E. V. Buzaneva and A. D. Gorchinskiy, *Chem. Mater.*, 1999, **11**, 771–778.
27 W. S. Hummers and R. E. Offeman, *J. Am. Chem. Soc.*, 1958, **80**, 1339.
28 S. Wang, Q. Gao and J. Wang, *J. Phys. Chem. B*, 2005, **109**, 17281–17289.
29 Z. D. Wang, M. Yoshida and B. George, *Comput. Theor. Chem.*, 2013, **1017**, 91–98.
30 X. Wang, X. Li, L. Zhang, Y. Yoon, P. K. Weber, H. Wang, J. Guo and H. Dai, *Science*, 2009, **324**, 768–771.
31 S. Yang, L. Zhi, K. Tang, X. Feng, J. Maier and K. Müllen, *Adv. Funct. Mater.*, 2012, **22**, 3634–3640.
32 C. K. Chua, A. Ambrosi and M. Pumera, *J. Mater. Chem.*, 2012, **22**, 11054–11061.
33 C. H. Choi, M. W. Chung, S. H. Park and S. I. Woo, *Phys. Chem. Chem. Phys.*, 2013, **15**, 1802–1805.
34 M. D. Stoller, S. Park, Y. Zhu, J. An and R. S. Ruoff, *Nano Lett.*, 2008, **8**, 3498–3502.
35 Y. Chang, F. Hong, C. He, Q. Zhang and J. Liu, *Adv. Mater.*, 2013, **25**, 4794–4799.
36 W. Ding, Z. Wei, S. Chen, X. Qi, T. Yang, J. Hu, D. Wang, L.-J. Wan, S. F. Alvi and L. Li, *Angew. Chem., Int. Ed.*, 2013, **52**, 11755–11759.
37 H. Wang, T. Maiyalagan and X. Wang, *ACS Catal.*, 2012, **2**, 781–794.
38 D. Zhang, Y. Hao, L. Zheng, Y. Ma, H. Feng and H. Luo, *J. Mater. Chem. A*, 2013, **1**, 7584–7591.
39 Z. Yang, Z. Yao, G. Li, G. Fang, H. Nie, Z. Liu, X. Zhou, X. a. Chen and S. Huang, *ACS Nano*, 2011, **6**, 205–211.
40 J. P. Paraknowitsch, A. Thomas and J. Schmidt, *Chem. Commun.*, 2011, **47**, 8283–8285.
41 Y. Dong, H. Pang, H. B. Yang, C. Guo, J. Shao, Y. Chi, C. M. Li and T. Yu, *Angew. Chem., Int. Ed.*, 2013, **52**, 7800–7804.
42 Z. Liu, H. Nie, Z. Yang, J. Zhang, Z. Jin, Y. Lu, Z. Xiao and S. Huang, *Nanoscale*, 2013, **5**, 3283–3288.
43 K. N. Kudin, B. Ozbas, H. C. Schniepp, R. K. Prud'homme, I. A. Aksay and R. Car, *Nano Lett.*, 2007, **8**, 36–41.
44 H. Liu, Y. Liu and D. Zhu, *J. Mater. Chem.*, 2011, **21**, 3335–3345.
45 X. Li, H. Wang, J. T. Robinson, H. Sanchez, G. Diankov and H. Dai, *J. Am. Chem. Soc.*, 2009, **131**, 15939–15944.

46 Y. Hernandez, V. Nicolosi, M. Lotya, F. M. Blighe, Z. Sun, S. De, I. T. McGovern, B. Holland, M. Byrne, Y. K. Gun'Ko, J. J. Boland, P. Niraj, G. Duesberg, S. Krishnamurthy, R. Goodhue, J. Hutchison, V. Scardaci, A. C. Ferrari and J. N. Coleman, *Nat. Nanotechnol.*, 2008, **3**, 563–568.
47 A. C. Ferrari, J. C. Meyer, V. Scardaci, C. Casiraghi, M. Lazzeri, F. Mauri, S. Piscanec, D. Jiang, K. S. Novoselov, S. Roth and A. K. Geim, *Phys. Rev. Lett.*, 2006, **97**, 187401.
48 I.-Y. Jeon, H.-J. Choi, S.-M. Jung, J.-M. Seo, M.-J. Kim, L. Dai and J.-B. Baek, *J. Am. Chem. Soc.*, 2012, **135**, 1386–1393.
49 A. I. Popov and D. H. Geske, *J. Am. Chem. Soc.*, 1958, **80**, 1340–1352.
50 S. Das, P. Sudhagar, V. Verma, D. Song, E. Ito, S. Y. Lee, Y. S. Kang and W. Choi, *Adv. Funct. Mater.*, 2011, **21**, 3729–3736.
51 M. J. Ju, I.-Y. Jeon, J. C. Kim, K. Lim, H.-J. Choi, S.-M. Jung, I. T. Choi, Y. K. Eom, Y. J. Kwon, J. Ko, J.-J. Lee, H. K. Kim and J.-B. Baek, *Adv Mater.*, 2014, **26**, 3055–3062.
52 L. Zhang and Z. Xia, *J. Phys. Chem. C*, 2011, **115**, 11170–11176.